



Geometric morphometrics shows a close relationship between the shape features, position on thalli, and CaCO₃ content of segments in *Halimeda tuna* (Bryopsidales, Ulvophyceae)

Jiri Neustupa · Yvonne Nemcova

Received: 15 September 2021 / Revised: 3 February 2022 / Accepted: 28 March 2022 / Published online: 18 April 2022
© The Author(s), under exclusive licence to Springer Nature Switzerland AG 2022

Abstract Calcifying green algae of the genus *Halimeda* J.V. Lamouroux are typical for the modular thalli composed of serial segments. Their CaCO₃ content gradually increases with age due to calcification, the intensity of which is largely linked to photosynthesis. The dynamics of segment phenotypic plasticity at different scales and its relation to CaCO₃ content is not well known. We investigated the populations of *Halimeda tuna* in the upper sublittoral of four regions on the Adriatic Sea coast. Using geometric morphometrics, we explored the patterns of segment shape plasticity, their relationships with the spatial factors and CaCO₃ content. The results showed that segment position on thalli was the main determinant of their shape features. This effect was considerably more prominent than the differences among plants, populations, or regions. Likewise, the segment shape proved to be a significant predictor of their CaCO₃ content. Segments with inversely conical shapes, typical for the lower parts of branches, contained significantly less CaCO₃ than the reniform and

oval segments that probably contribute most to the overall carbonate budget of the Mediterranean *Halimeda* draperies.

Keywords Calcifying algae · Geometric morphometrics · Green algae · *Halimeda tuna* · Phenotypic plasticity · Ulvophyceae

Introduction

Marine green algae classified into the genus *Halimeda* J.V. Lamouroux are one of the most important global producers of inorganic carbonate sediments (Hillis, 1991; Rees et al., 2007; Davies, 2011). The above-ground parts of their macroscopic thalli are composed of serial sequences of segments joined by relatively narrow nodes (Hillis-Colinvaux, 1980). New segments arise from the decorticated parts located along the margins of mature segments. Thus, each segment is necessarily younger than those located beneath in a series forming a single branch. However, the age differences among segments forming a single branch are not necessarily linear because individual segments or entire branches may be repeatedly shed during the vegetative growth phase of plants (Drew, 1983; Ballesteros, 1991a). Precipitation of aragonite microcrystals takes place in the intertricular spaces (IUS) and among the medullar filaments within segments. The CaCO₃ content gradually increases with segment age until most of these spaces are filled in, and most of

Handling editor: Iacopo Bertocci

Supplementary Information The online version contains supplementary material available at <https://doi.org/10.1007/s10750-022-04876-y>.

J. Neustupa (✉) · Y. Nemcova
Department of Botany, Faculty of Science, Charles University Prague, Prague, Czech Republic
e-mail: neustupa@natur.cuni.cz

the segment dry weight is formed by the inorganic CaCO_3 (Prát & Hamáčková, 1946; Wizemann et al., 2014; Peach et al., 2017). Calcification is closely connected with photosynthesis that elevates pH of the calcification fluid within the IUS and, thus, facilitates aragonite precipitation (Borowitzka & Larkum, 1987; McNicholl et al., 2019). Consequently, variation in the calcification rates among *Halimeda* plants within populations is known to be related to the differences in the light availability (Stark et al., 1969; Pongparadon et al., 2020). While the CaCO_3 content of the entire thalli was reported many times for multiple *Halimeda* species (Böhm, 1973; Hillis-Colinvaux, 1980; Peach et al., 2017), considerably less data are available for different thallus parts or even individual segments (Borowitzka & Larkum, 1976; van Tussenbroek & van Dijk, 2007). Likewise, there are virtually no data on any possible relation between morphological characteristics of individual segments, such as their shape and size, and the overall spatial capacity that is available for CaCO_3 precipitation, which might then be manifested by differences in their mineral content.

The segments forming a single individual obviously share the same genome, and they are joined by siphonous nodal filaments without any cross-cell walls. However, their shapes and sizes are often profoundly plastic (Vroom et al., 2003; Pongparadon et al., 2017). Especially in the erect species, segments deviating from the species-specific shapes are often formed in the basal parts of the thalli (Verbruggen et al., 2005). At the same time, the immature apical segments also often lack the typical shape features of their respective *Halimeda* species (Verbruggen et al., 2005). In addition, several key environmental factors, such as light availability (Yñiguez et al., 2010; Pongparadon et al., 2020), nutrients (Smith et al., 2004), or wave exposure (Kooistra & Verbruggen, 2005; Pongparadon et al., 2017), were found to be correlated with plastic changes of segments. In particular, *Halimeda* plants growing in shaded habitats often develop comparatively larger segments than those in the highly irradiated localities (Vroom et al., 2003; Pongparadon et al., 2020). In addition, the smaller plants of multiple *Halimeda* species from exposed habitats are also typical for distinctly different segment shapes in comparison with plants growing in deeper and sheltered habitats (Verbruggen et al., 2006). This suggests an allometric relationship between the shape and size

of segments acting as a basic mechanism of the plastic response of *Halimeda* species to environmental heterogeneity.

In fact, static morphological allometry, i.e. shape-to-size relation of mature segments, was recently identified as the key feature of their morphospace structure in Mediterranean *Halimeda tuna* (J. Ellis & Solander) J.V. Lamouroux (Neustupa & Nemcova, 2018). The species was characterized by reniform to oval shapes of the mature segments (Hillis-Colinvaux, 1980). However, two populations from the Northern Adriatic Sea also included a substantial proportion of smaller segments with more elongated shapes that often occurred on the same plants as the reniform segments. In addition, these populations growing at the same depth in the upper sublittoral significantly differed in the mean shape of their segments, indicating that local factors might have influenced their morphogenesis (Neustupa & Nemcova, 2018).

In the Mediterranean Sea, *H. tuna* is the only native species of the genus. The thalli of this species is typically attached to the hard substrates of the Mediterranean sublittoral habitats by irregularly shaped holdfasts. The ramified branches made of flattened segments often form dense draperies on steep rock surfaces and significantly contribute to benthic CaCO_3 production in the Mediterranean Sea (Ballesteros, 1991a; Canals & Ballesteros, 1997). In the pronounced seasonal climatic conditions of the warm temperate Mediterranean Sea, the populations of *H. tuna* typically produce the highest number of new segments during spring and summer. At the end of the summer season, the plants usually consist of the highest number of segments, which are eventually shed during the late autumn and winter periods (Ballesteros, 1991b; Llobet et al., 1991). However, it should be noted that branches of *H. tuna* in the Mediterranean Sea usually consist of a considerably smaller number of segments than the tropical taxa (Hillis-Colinvaux, 1980; Llobet et al., 1991). For example, at the end of the summer season, the Northern Adriatic populations of the species typically only consisted of about 9–10 serial segments within a single branch (Neustupa & Nemcova, 2018).

The present study is focused on the shape and size variation of *H. tuna* segments in the upper sublittoral of multiple localities across the Adriatic Sea in relation to their CaCO_3 content. Geometric morphometrics of the segment outlines are used to illustrate the

structure of the morphospace illustrating their shape variation. In addition, the microscale differentiation of segments within individual plants is quantified and compared to the differences among populations and regions. How much of the shape variation among segments is explained by their varying position within individual branches rather than by differentiation among populations and regions? In addition, we aim to detect shape and size characteristics of segments that are linked to their CaCO_3 content. Which factors will prove to be decisive for the variation in CaCO_3 content among segments? Are there any consistent differences in this key feature of *Halimeda* segments related to their position on thalli, as well as their size and shape characteristics? These questions are tackled by combination of the geometric morphometric analyses and the CaCO_3 content measurements of *H. tuna* segments from four regions across the Adriatic Sea.

Materials and methods

Sampling

Thalli of *H. tuna* were sampled on October 15–23, 2019 at 12 sites located in four regions along the Eastern coast of the Adriatic Sea (Fig. 1a; Online Resource 1, Table S1). The geographical distance

among these regions is more than 500 kms and their ecological conditions differ, especially in terms of the sea surface temperature (SST) across the season. The northernmost populations in the Gulf of Trieste are typical for the annual SST about 16.0 to 17.5°C. In contrast, the 3 more southerly regions in the central and southern Adriatic Sea reach the average annual SST around 18.5 to 19.5°C (Bonacci et al., 2021). However, average SST during the peak growing season (June to September) lack any latitudinal gradient across the investigated region, reaching the maximum levels of 23 to 26°C (Pastor et al., 2018).

At each site, seven plants were sampled in the upper sublittoral from the 30×30 cm squares on the north-facing vertical rocks at 100–150 cm depth. The segments composing the longest available series within each plant were carefully separated, pressed on an absorbent paper, and scanned. Occasional uncalcified apical segments with unfinished morphogenesis were omitted from the subsequent analyses. The final dataset consisted of 535 segments from 84 different plants originating from 12 populations.

Mineral content of segments

Individual segments were dried at 60°C and weighed using a precision balance (LB-1050/2, Laberte, Hungary) until constant weight was achieved. Segments

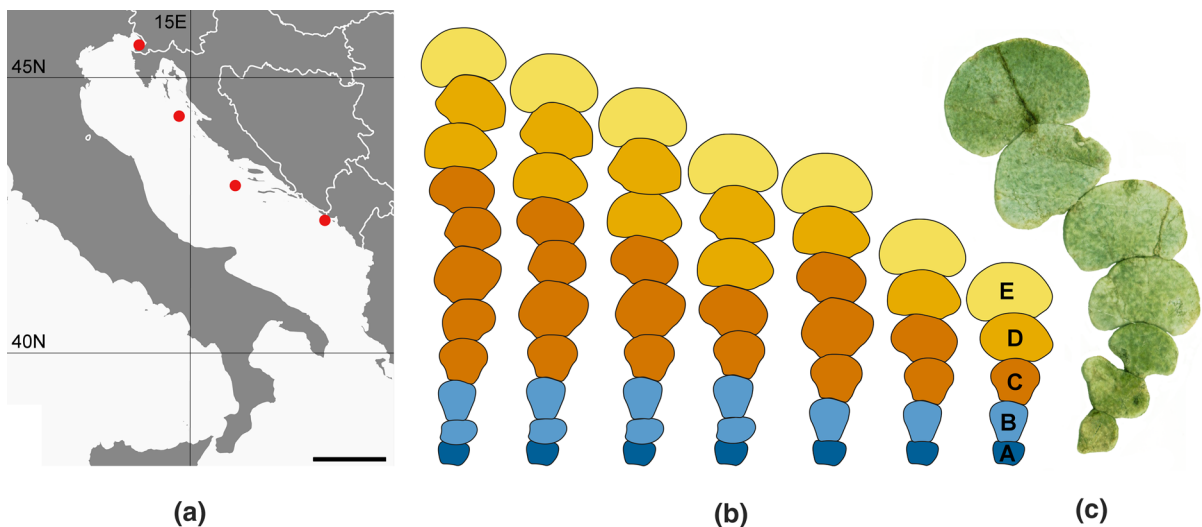


Fig. 1 (a) Position of 4 sampled regions along the eastern coast of the Adriatic Sea. Scale bar=200 km. (b) Designation of position levels along the branches of *H. tuna* varying from 5

to 11 segments. The signs A–E correspond to boxplot designations in Fig. 3. (c) A single *H. tuna* plant consisting of 7 serial segments

were decalcified by immersion in the 5% HCl solution for 10 min or until bubbling had ceased (Vroom et al., 2003). The decalcified segments were rinsed with distilled water, dried at 60°C to constant weight, and weighed using a precision balance. The proportional mineral content of each segment was determined as $C = 1 - dcw/drw$, where drw is the total dry weight and dcw is the dry weight after decalcification. The data on segment dry weight and their CaCO_3 content are available online (Online Resource 1, Table S2).

Geometric morphometrics

The two-dimensional projections of the segment forms were registered by a series of 80 equidistant points located along their margins. The starting point of each outline was located at the basal node position. This point was treated as the sole fixed landmark in the generalized Procrustes analysis (GPA). The remaining 79 points were considered sliding landmarks of which initial position was solely defined by their equidistant placement along the segment outline. The points were digitized using the semi-automated *background curves* tool implemented in TpsDig, ver. 2.22 (Rohlf, 2015). To quantify the effect of measurement error on the observed shape variation, each segment was digitized four times. Each of the two co-authors digitized the entire dataset twice. First, the segment outlines were registered clockwise then they were registered counter-clockwise and relabelled to match the order of the clockwise digitization. Thus, the final dataset for the geometric morphometric analysis consisted of $4 \times 535 = 2140$ configurations of two-dimensional outline points. These coordinates are available online at <http://doi.org/10.5281/zenodo.5504135>.

In this study, the shape analysis only involved the variation among segments. Thus, shape asymmetry between their two halves was not considered. As these two halves of *Halimeda* segments are essentially unsigned, their left or right position cannot be determined among different plants (Neustupa & Nemcova, 2018; 2020). Thus, the shapes of the two symmetric halves of each segment were averaged. This was based upon reflection of the configurations across their axis of bilateral symmetry, relabelling the paired points from the opposite halves, and averaging these original and mirrored configurations of each segment in the GPA (Klingenberg et al., 2002). GPA also

involved semilandmark sliding along the tangents to the outline curve, in order to assure optimal correspondence of individual outlines to the mean configuration by minimizing the bending energy between each configuration and the consensus shape (Perez et al., 2006; Gunz & Mitteroecker, 2013). The function *gpa* implemented in the R package *geomorph*, ver. 3.3.1 (Adams & Otárola-Castillo, 2013; R Core Team, 2020), was used for these analyses. Segment size was evaluated by their area yielded by the function *polyarea* in the R package *geometry*, ver. 0.4.5 (Habel et al., 2019). The log-transformed area values were used in the subsequent analyses to ensure their optimum linear relationship with the other variables.

Statistical analysis

Symmetrized configurations aligned by GPA were subjected to principal component analysis (PCA). Resulting principal components (PCs) were used to illustrate the most prominent patterns of segment shape variation. The function *gpa* of the package *geomorph*, ver. 3.3.1, was used for these analyses. The segment shapes characterizing the marginal occupied positions of the morphospace spanned by individual PCs were visualized in TpsRelw, ver. 1.65 (Rohlf, 2015).

The relative strength of spatial factors and the position of segments on thalli on their shape features were evaluated by the multivariate type I non-parametric permutational analysis of variance (ANOVA). The analysis decomposed the matrix of Procrustes distances among individual segments into different sources corresponding to the independent factors and their interactions. Thus, the matrix of tangent Procrustes distances was partitioned across the different sources of variation (factors) by fitting a linear model. It should be noted that the multivariate permutational ANOVA with a balanced factorial design is very robust to heterogeneity of multivariate dispersions (Anderson & Walsh, 2013). In addition, resampling statistics (permutations) that does not assume normality (Anderson, 2017) and is not affected by the high dimensionality of the shape data (Cardini et al., 2015), was used to assess the probabilities of individual null hypotheses assuming the absence of any relationships between the Procrustes distance matrix of the dependent variables and the explanatory factors. The model yielded the Procrustes sum of squares

(SS) spanned by each factor and their percentage proportion on the total variation evaluated by the coefficient of determination (η^2). In addition, we also tested for the significance of the effects by comparing their original Procrustes SS values with the distribution of random SS yielded by 999 permutations (Schaefer et al., 2006).

The permutation design reflected the nested structure of the spatial factors. Thus, the factor ‘region’ that accounted for the differentiation among the segments sampled in four different regions along the Adriatic Sea coast was evaluated by comparison with the random SS distribution yielded by re-shuffling of individual sites then the shape differences of segments due to variation among sites were tested against the distribution of SS values yielded by repeated evaluation of random ‘site’ factors created by re-shuffling of plants. Likewise, the Procrustes SS spanned by shape variation at the level of individual plants were evaluated against the random distribution obtained by re-shuffling of segments among plants. The main fixed effect of ‘position’ was coded as the categorical variable with 5 levels that corresponded to the relative position of each segment on their respective plants. The analysed branches consisted of 5 to 11 segments and the assignment of individual segments into one of the ‘position’ levels reflected this variation (Fig. 1b). The lowest level always included only the basal segment of each branch developed immediately above the holdfast. Likewise, the single upper-most mature segment was consistently classified into the 5th ‘position’ level. There were 1 or 2 suprabasal and subapical segments positioned immediately above the basal segment and below the apical segment, respectively. Finally, a varying number of segments in the middle part of the branches were classified into the intermediate positional class. The Procrustes SS spanned by this factor were evaluated by their comparison with the random SS distribution created by repeated re-shuffling of the segments among their positional levels.

The interactions of ‘position’ effect with the nested factors were tested by randomization of segment positions within the levels of each respective spatial effect. The interaction of ‘position’ and ‘region’ factors evaluated the differences in the variation of segment shapes due to their position on branches among the regions. Likewise, two other interaction effects quantified similar differences among sites and individual

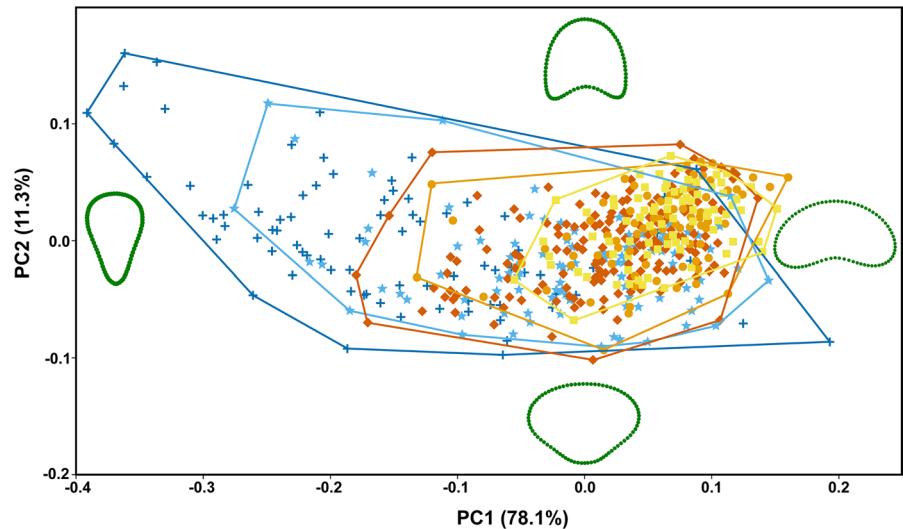
plants. The effects of spatial factors and position of segments on their dry weight, mineral content, and log area were tested by three separate univariate ANOVA models. The effects of the independent factors were evaluated in the analogous design as in the multivariate model focused on decomposition of the shape variation. However, as the decalcification of segments is obviously a one-way process, dry weight and mineral content of segments were measured without any independent repetitions. Thus, these models did not include any evaluation of measurement error. All four models were run in R, ver. 4.0.2, using the function *procD.lm* implemented in the package *geomorph*, ver. 3.3.1. The R script for these analyses is available online at <http://doi.org/10.5281/zenodo.5504135>.

Relationships among the univariate parameters of segments, such as their dry weight, mineral content, log area, and the most prominent shape dynamics spanned by PC1, were compared by a series of linear correlation analyses. In addition, the partial linear correlation analyses evaluating the relationships between each pair of these univariate variables while controlling for the effects of two remaining variables were also conducted. Significance levels of the permutational p values resulting from these analyses were adjusted for multiple comparisons using the Bonferroni correction (Perrett & Mundfrom, 2010). These analyses were conducted in PAST, ver. 4.04 (Hammer et al., 2001).

Results

PCA of the segment shape data illustrated that most of the variation (78.1%) was concentrated into a single dimension spanned by PC1 (Fig. 2). The underlying shape trend highlighted the variation between the broadly reniform segments with the positive PC1 scores and those with elongated, inversely conical shapes in the opposite parts of the PC1 gradient. The second most important trend in the shape variation, illustrated by PC2 (11.3%), showed the differences between segments with basal stalks in the negative parts of this axis and those typical for rather concave basal outlines with the positive PC2 scores. Projection of the positions of individual segments into the morphospace defined by PC1 and PC2 illustrated that virtually all segments with inversely conical shapes

Fig. 2 PCA ordination plot of the segment shape data showing first two PCs (PC1 vs. PC2). The configurations illustrate shapes typical for the most marginal occupied positions on each PC. Colours correspond to positions of segments on branches illustrated in Fig. 1a



were those located in the basal and suprabasal parts of their thalli. Conversely, the segments located in the upper parts of branches were typical for oval and reniform shapes (Fig. 2).

The Procrustes ANOVA model also illustrated the prominent effect of position on the shape of analysed segments (Table 1). This single factor with five levels, describing different positions of segments on branches, explained 35.2% of the total shape variation. Conversely, the spatial factors proved to be comparatively less important for the observed variation in segment shapes. Differentiation among the regions only spanned 1.9% of the variation and the localities within regions only accounted for an additional 2.9%. Contrary to variation among the regions, the factor

'locality' proved to be significant against the random SS distribution. Shape variability that was averaged at the level of 84 studied plants nested within localities explained 9.9% of the total variation in the dataset. This effect also proved to be significantly higher than the randomly obtained SS values for this effect. The obtained values for the interaction effects among the position and the spatial factors showed that different position of segments on thalli did not differ among the regions and localities. Conversely, there were obvious differences in the 'position' effect among the plants. This interaction described 30.8% of the total shape variation. However, the relatively low mean squares (MS) for this effect, which were comparable to those obtained for the other two interaction factors,

Table 1 Results of multivariate analysis of variance (ANOVA) decomposing variation in segment shape into different sources

Source of variation	df	SS	MS	η^2	<i>P</i>
Position	4	11.188	2.7969	0.352	0.001
Region	3	0.633	0.2111	0.019	0.208
Locality (region)	8	0.918	0.1147	0.029	0.005
Plant (locality)	72	3.142	0.0436	0.099	0.007
Position:region	12	0.562	0.0468	0.018	0.061
Position:region:locality	32	0.975	0.0305	0.031	0.581
Position:region:locality:plant	288	9.794	0.0340	0.308	0.016
Measurement error—person	420	1.052	0.0025	0.033	
Measurement error—direction	420	0.222	0.0005	0.007	
Measurement error—person:direction	420	0.196	0.0005	0.006	
Residuals	460	3.126	0.0068	0.098	
Total	2139	31.808			

df degrees of freedom, *SS* sum of squares, *MS* mean squares, η^2 coefficient of determination, *p* probability of the null hypothesis

indicated that the strength of these differences did not constitute a prominent feature of the overall shape variation. Likewise, the components of the measurement error were relatively very small compared to the evaluated independent factors (Table 1).

Relationship of segment size with the independent factors largely followed a similar pattern as the shape data (Table 2). There was a prominent effect of segment position explaining 44.4% of the total variation.

The segments located in the lower parts of the thalli were usually considerably smaller than those occurring in the middle and upper portions (Fig. 3a). Among the spatial factors, the differences among the regions and localities were relatively very small and they were not significant in the randomization tests. Conversely, size differentiation of segments among plants described 11.3% of the variation, and this effect was large enough to yield a very low p value = 0.002.

Table 2 Results of permutational ANOVA decomposing size variation of *H. tuna* segments into different sources

Source of variation	Df	SS	MS	η^2	P
Position	4	92.065	23.0162	0.444	0.001
Region	3	2.275	0.7583	0.011	0.358
Locality (region)	8	4.862	0.6078	0.023	0.098
Plant (locality)	72	23.326	0.3240	0.113	0.002
Position:region	12	4.936	0.4114	0.024	0.007
Position:region:locality	32	6.908	0.2159	0.033	0.197
Position:region:locality:plant	288	46.098	0.1601	0.222	0.949
Measurement error—person	420	1.517	0.0036	0.007	
Measurement error—direction	420	0.020	0.0001	0.000	
Measurement error—person:direction	420	0.029	0.0001	0.000	
Residuals	460	25.166			
Total	2139	207.202			

df degrees of freedom, *SS* sum of squares, *MS* mean squares, η^2 coefficient of determination, *p* probability of the null hypothesis

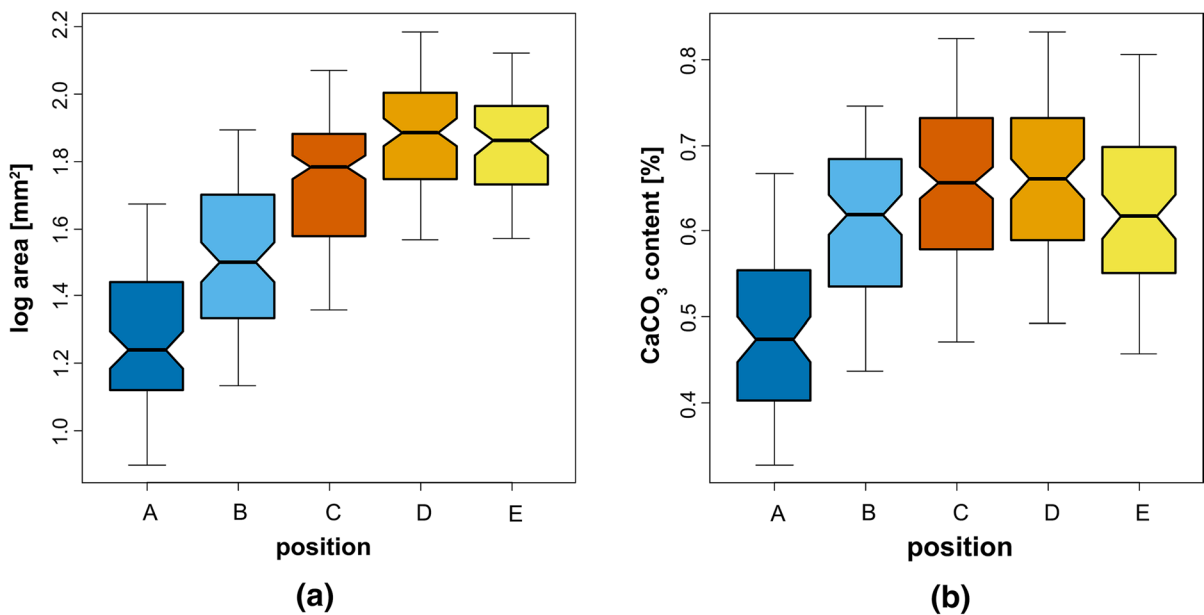


Fig. 3 Comparison of five position levels of *H. tuna* segments on branches and (a) segment log area and (b) their CaCO_3 content. Colours correspond to positions of segments on branches

illustrated in Fig. 1a. Whiskers illustrate the upper and lower quartiles and notches estimate the 95% confidence intervals of the median values

Table 3 Results of permutational ANOVA decomposing variation in CaCO₃ content of *H. tuna* segments into different sources

Source of variation	Df	SS	MS	η^2	<i>P</i>
Position	4	1.782	0.4454	0.225	0.001
Region	3	0.673	0.2243	0.085	0.129
Locality (region)	8	0.690	0.0862	0.087	0.003
Plant (locality)	72	1.592	0.0221	0.201	0.001
Position:region	12	0.425	0.0354	0.054	0.001
Position:region:locality	32	0.188	0.0059	0.024	0.573
Position:region:locality :plant	288	2.112	0.0073	0.267	0.001
Residuals	115	0.449			
Total	534	7.911			

df degrees of freedom, *SS* sum of squares, *MS* mean squares, η^2 coefficient of determination, *p* probability of the null hypothesis

Table 4 Results of permutational ANOVA decomposing variation in dry weight of *H. tuna* segments into different sources

Source of variation	Df	SS	MS	η^2	<i>P</i>
Position	4	918.4	229.6	0.062	0.001
Region	3	422.3	140.8	0.028	0.439
Locality (region)	8	1033.1	129.1	0.069	0.038
Plant (locality)	72	3797.3	52.7	0.256	0.001
Position:region	12	367.5	30.6	0.025	0.108
Position:region:locality	32	553.8	17.3	0.037	0.598
Position:region:localit y:plant	288	4802.1	16.7	0.324	0.936
Residuals	115	2939.7			
Total	534	14,834.3			

df degrees of freedom, *SS* sum of squares, *MS* mean squares, η^2 coefficient of determination, *p* probability of the null hypothesis

The effects of different position of segments on thalli significantly differed among the studied regions but not among the localities and plants.

The effects of segment position on their dry weight and the CaCO₃ content (Tables 3, 4) were less prominent than in the shape and size datasets. In both cases, the relationships were significant, but they only explained 22.5% of the variation in the CaCO₃ content and 6.2% in the dry weight of segments. The average CaCO₃ content of the analysed segments across the entire dataset was 61.6% [95% CI: 60.6, 62.7]. The effect of position on the CaCO₃

content was largely due to the considerably lower values of the segments classified in the two lowest classes (Fig. 3b). While mean CaCO₃ content of the suprabasal segments was only 48.9% [46.5, 51.3] of their total dry weight, it was 60.7% [58.7, 62.7] for the segments located immediately above them in the 'B' position (Figs. 1b, 3b) then the values for the segments in the middle and subapical sections of thalli were comparatively higher with 65.2% [63.7, 66.7] and 66.0% [63.9, 68.1], respectively. Finally, there was a slight decrease in the apical mature segments with average 63.0% [60.4, 65.6] of their dry weight being formed by the inorganic CaCO₃. The effect of the nested spatial factors on the segment dry weight and the CaCO₃ content was limited, but significant differences in both these variables were detected at the level of localities and individual plants. Likewise, the effect of segment position on their dry weight and the CaCO₃ content clearly differed among the analysed plants as shown by relatively high SS values of this interaction effect in both these ANOVA models (Tables 3, 4).

Dry weight of segments proved to be moderately correlated with their CaCO₃ content ($r=0.49$; Table 5; Fig. 4a). Both dry weight and the CaCO₃ content were significantly correlated with the single most prominent shape pattern represented by PC1. In particular, the inversely conical segments, typical for the negative margins of PC1, generally had lower CaCO₃ content than those with the oval and reniform shapes ($r=0.43$; Table 5; Fig. 4b). A significant linear relationship between the CaCO₃ content and PC1 was retained even after the effects of dry weight and segment size were taken into account by the partial linear correlation analysis (Table 5). On the other hand, the partial linear correlation between dry weight of segments and PC1 proved to be insignificant. A significant linear relationship was also detected between the segment size and PC1 ($r=0.64$; Table 5; Fig. 4c). In this case, it was shown that the inversely conical segments were usually smaller than those with the reniform or oval shapes. This relationship remained strongly significant even after the effects of dry weight and the CaCO₃ content of segments were taken into account (Table 5). Finally, the positive linear relationship between the CaCO₃ content and log area of segments proved to be fully explained by covariation of these factors with the shape pattern of PC1 and dry weight (Table 5).

Table 5 Results of the linear correlation analyses and the partial linear correlation analyses among the characteristics of *H. tuna* segments

Linear correlation	Pearson's <i>r</i>	<i>P</i>
Log segment area vs. % CaCO ₃	0.422	0.0001
Log segment area vs. total dry weight	0.639	0.0001
Log segment area vs. segment shape [PC1]	0.637	0.0001
% CaCO ₃ vs. total dry weight	0.485	0.0001
% CaCO ₃ vs. segment shape [PC1]	0.425	0.0001
Total dry weight vs. segment shape [PC1]	0.378	0.0001
Partial linear correlation	<i>r</i>	<i>P</i>
Log segment area vs. % CaCO ₃	0.001	0.9753
Log segment area vs. total dry weight	0.526	0.0001
Log segment area vs. segment shape [PC1]	0.537	0.0001
% CaCO ₃ vs. total dry weight	0.329	0.0001
% CaCO ₃ vs. segment shape [PC1]	0.251	0.0001
Total dry weight vs. segment shape [PC1]	-0.127	0.0034

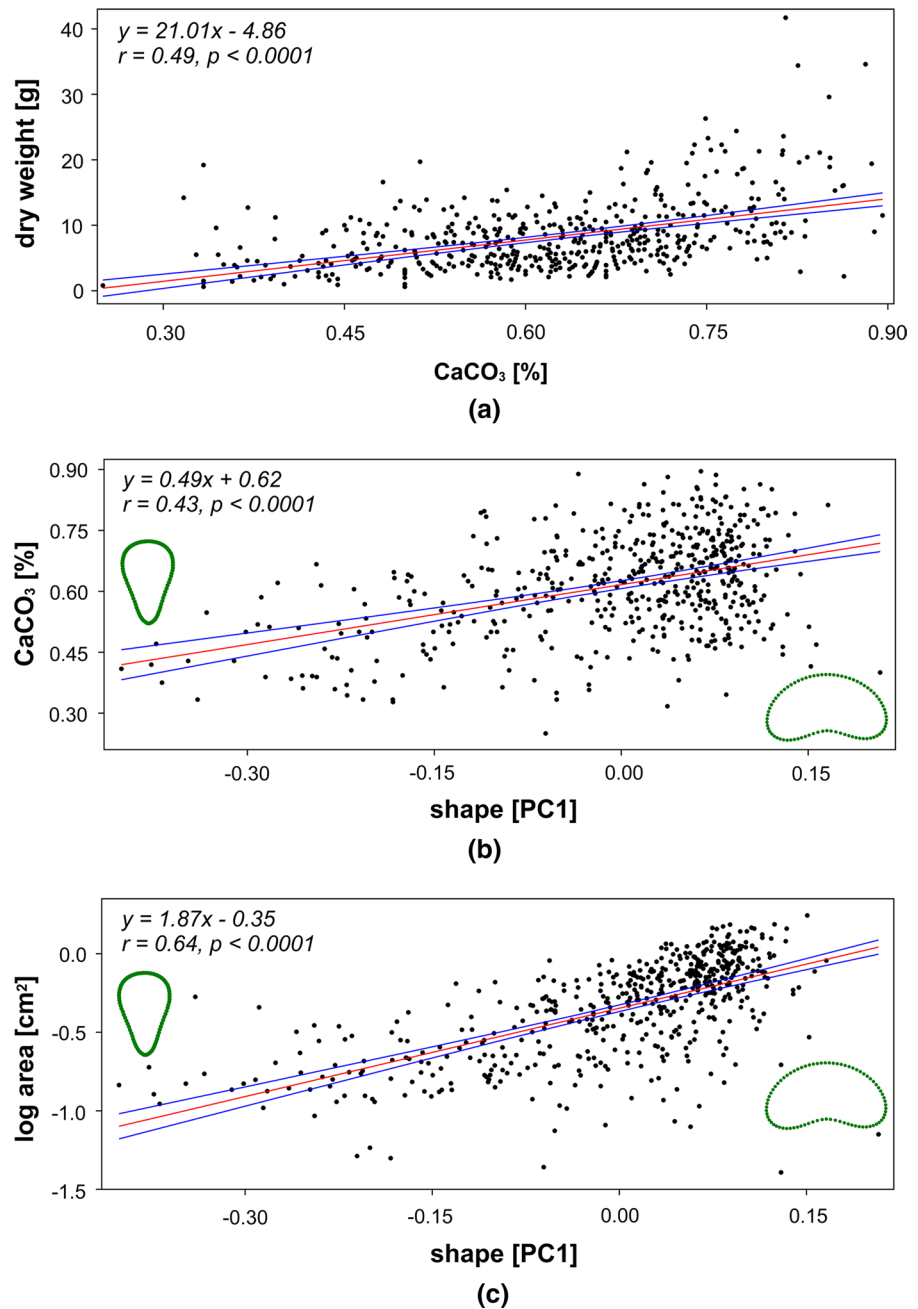
Significant *P* values are depicted in bold

Discussion

The spatial factors did not markedly contribute to the observed shape and size variation of *H. tuna* segments. However, the meso- and microscale differentiation at the level of individual populations and plants still was more important than the presumed differences among 4 sampled regions. In fact, the observed pattern in the morphometric data showed that quantitative differences in segment shape and size of *H. tuna* in the Adriatic Sea were only detectable at the level of individual populations or plants. According to recently published phylogeographic data, *H. tuna* in the Adriatic Sea consists of a single haplotype (Rindi et al., 2020). Morphometric homogeneity of the segments in 4 regions located across the Adriatic Sea showed that the large-scale ecological factors, such as the minimum SST, were not major factors in the variation of the shape and size features of this haplotype. The situation was somewhat different for individual populations within regions and individual plants. Here, we detected significant differences in segment shape and, in the case of individual plants, also in segment size. Although individual populations were collected to minimize major environmental differences, such as depth or directional exposure, it is possible that local heterogeneity in the environment at the microscale led to some non-random differentiation in segment shape and size.

In general, the structure of the segment shape variation within the dataset spanning the gradient of about 513 km across the Adriatic Sea showed remarkable similarity to the results of similar analyses of much smaller local *H. tuna* populations. The shape changes described by the two most important PCs were virtually identical to those obtained in the two earlier geometric morphometric studies of this species (Neustupa & Némecová, 2018, 2020). This means that the shape trends illustrated by these PCs represent essentially ubiquitous and deeply conserved plasticity patterns of this species. The allometric dynamics spanned by PC1, which constituted a substantial part of the observed shape variation of segments, was closely linked to their different positions on plants. This effect also proved to be the single most important factor explaining the observed shape and size variation in the ANOVA models. In general, the segments in the lower parts of the plants were much more typical for their inversely conical shapes and smaller sizes than those in the middle and apical parts of thalli. The lower segments are, in most cases, deviated from the reniform shapes. Conversely, position of individual segments within the morphospace clearly illustrate that the inversely conical shapes were practically absent from the upper parts of thalli. The higher abundance of segments deviating from the typical, species-specific shapes in the basal parts of the thalli was already shown by Verbruggen et al.

Fig. 4 Linear correlation analyses of (a) segment dry weight and their CaCO_3 content, (b) CaCO_3 content and the single most prominent shape trend spanned by PC1, and (c) log area of segments and the shape trend spanned by PC1. The configurations illustrate shapes typical for the most marginal occupied positions on PC1. The Pearson's r and permutation p values are depicted. The 95% confidence intervals are shown by blue lines



(2005), who also noted that this phenomenon is predominantly associated with erect species, such as *H. tuna*, but does not occur in taxa with sprawling thalli. Thus, it seems that the observed morphological deviations of the segments located in the lower parts of thalli can be interpreted as a morphological adaptation providing the mechanical support for the younger reniform and oval segments in the middle and apical

parts of branches. However, it should be emphasized that this mechanical support of the thalli is based solely on the shape changes of segments, not on their higher encrustation with CaCO_3 . By contrast, higher mineral content was typical for the reniform and oval segments found in the middle and apical parts of branches that produce most of the inorganic CaCO_3 within the studied populations.

In general, the average CaCO_3 content of 61.6% was more or less in line with previously recorded values for *H. tuna* in the Mediterranean Sea (Prát & Hamáčková, 1946; Ballesteros, 1991a; Bilgin & Ertan, 2002). Interestingly, the comparatively lower values of 59.7% (Prát & Hamáčková, 1946) and 45.7% (Ballesteros, 1991a) were recorded for the populations from deeper habitats of the middle and lower sublittoral. Conversely, the relatively high values of 68.1% CaCO_3 were reported for *H. tuna* populations growing in the upper sublittoral region (Bilgin & Ertan, 2002), similar to those analysed in the present study. The differences in CaCO_3 content among the 4 studied regions did not significantly contribute to the observed variation in this key feature of segments. Thus, we can see that similar to the morphometric characteristics, calcification rates were likely not influenced by the seasonal SST gradient within the Adriatic Sea. Apparently, most of the calcification in segments of Mediterranean *H. tuna* takes place during the spring and summer vegetative seasons (Ballesteros, 1991a). During this part of the year, the SSTs across the basin are relatively homogenous (Pastor et al., 2018), and the pronounced latitudinal gradient in the February minimum SST values does not influence the CaCO_3 content of the populations. The average values of CaCO_3 proportion on total dry weight of segments were clearly lower than similar measurements of the tropical *Halimeda* species (Böhm, 1973; Hillis-Colinvaux, 1980; Ortegón-Aznar et al., 2017; Carneiro et al., 2018). Likewise, relatively low CaCO_3 values were also found in the warm temperate taxa from the *Halimeda cuneata* Hering complex in the southern hemisphere (Böhm, 1973). Thus, it is possible that comparatively lower CaCO_3 content of the extratropical *Halimeda* species is due to the relatively lower average temperature values of their environment, leading to relatively decreased overall photosynthetic productivity and calcification rates that yield comparatively lower mineral content of their thalli.

When we now take a closer look at our data on the characteristics of individual segments, we see that their dry weight was closely correlated with the CaCO_3 content. This shows that the increase in the segment dry weight is primarily due to their gradual calcification. Our data also showed a significant relationship between segment size, shape, and CaCO_3 content. In particular, the relationship between the

main shape trend described by PC1 and CaCO_3 content remained strongly significant in the partial linear correlation analysis even with the two size measures taken as covariates. Thus, these results suggest that the shape of the segments is a net morphological predictor of their CaCO_3 content, with the reniform segments having on average about 5 to 17 percentage points more of the CaCO_3 content on their dry weight than those with the inversely conical shapes. This difference is closely related to the different position of these segments on thalli.

The calcification rates of *Halimeda* segments are inherently linked to photosynthesis (Borowitzka & Larkum, 1987; Prathep et al., 2018). It was shown that up to 77% of the variation in *Halimeda* calcification can be explained by differences in the photosynthetic rates among plants (Jensen et al., 1985). Thus, it is possible that photosynthetic activity of inversely conical segments might be limited by their position in the lower parts of thalli, where they are shaded by younger reniform segments in a relatively dense stand of *Halimeda* draperies for most of their existence during the vegetative season. Then, the relatively lower CaCO_3 content of inversely conical segments might be related to their overall lower photosynthetic activity due to their prevailing position in the lower parts of branches leading to comparatively decreased calcification rates. However, this hypothesis would need to be tested by an analysis of the actual calcification rates among segments located in different parts of the thalli within the Mediterranean *Halimeda* draperies.

It should be noted that the observed relatively lower CaCO_3 content of the inversely conical segments was negatively related to their overall age. These segments, typically occurring in the lower portions of thalli, are necessarily older than the segments located above them. This finding is rather inconsistent with the relatively balanced CaCO_3 content values along the thalli (van Tussenbroek & van Dijk, 2007) or even a steady increase in the mineral proportion of older segments within tropical *Halimeda* populations (Barry et al., 2013). Interestingly, a very similar pattern of a relatively lower CaCO_3 content in the basal parts of the thalli was also found in extratropical *H. cuneata* (Böhm, 1973). Thus, it is possible that this phenomenon is preferentially manifested in *Halimeda* species occurring in the non-tropical regions, and it might possibly be related to lower aragonite saturation states (Ω) and higher solubility in these colder

environments (Mucci, 1983; Hall-Spencer & Harvey, 2019). These might lead to gradual dissolution of CaCO_3 during the colder parts of the season in older segments located in the basal parts of thalli resulting in their comparatively lower mineral content in comparison to the segments in the middle and subapical regions largely produced during the summer months with more suitable conditions for CaCO_3 accumulation (Ballesteros, 1991a). Therefore, the effects of the ongoing climate change on *Halimeda* populations in the Mediterranean will be most pronounced in terms of their carbonate budget through the production of segments with the reniform and oval shapes located in the middle and subapical parts of thalli. The influence of various abiotic and biotic factors related to the climate change in the Mediterranean ecosystems, such as heat waves, acidification, or increased herbivory by invasive species (Vergés et al., 2014), on their production, shape features and plasticity is, therefore, an intriguing aspect for future research of this key species of the Mediterranean macroalgae.

Summing up, the study showed that segment shape is a significant predictor of their CaCO_3 content in *H. tuna* from the Adriatic Sea. The plants typically include comparatively smaller segments with inversely conical shapes in the lower parts of thalli which usually contain significantly less CaCO_3 than those developed in the middle and apical portions. Thus, the production of these segments typical for the reniform or oval shapes is probably key to the overall carbonate budget of *H. tuna* populations in the Mediterranean ecosystems.

Acknowledgements The authors wish to thank the Ministry of the Sea, Transport, and Infrastructure of the Republic of Croatia for the field research permit no. 6422/2019/JLJ and Prof. Dr. Zrinka Ljubešić for her kind assistance in arranging the research permission. The study was supported by the institutional grant of Charles University ‘Progres Q43’.

Funding The study was supported by the institutional grant of Charles University ‘Progres Q43’.

Data availability Primary data used for the analyses are available online at: <http://doi.org/10.5281/zenodo.5504135>

Code availability The R scripts used for the analyses are available online at: <http://doi.org/10.5281/zenodo.5504135>

Declarations

Conflict of interest The authors declare that they have no conflict of interest.

References

- Adams, D. C. & E. Otárola-Castillo, 2013. geomorph: an R package for the collection and analysis of geometric morphometric shape data. *Methods in Ecology and Evolution* 4: 393–399.
- Anderson, M. J., 2017. Permutational multivariate analysis of variance (PERMANOVA). In Balakrishnan, N., T. Colton, B. Everitt, W. Piegorisch, F. Ruggeri & J. L. Teugels (eds), *Wiley StatsRef: Statistics Reference Online* Wiley, Oxford: 1–15. <https://doi.org/10.1002/9781118445112.stat07841>.
- Anderson, M. J. & D. C. I. Walsh, 2013. What null hypothesis are you testing? PERMANOVA, ANOSIM and the Mantel test in the face of heterogeneous dispersions. *Ecological Monographs* 83: 557–574.
- Ballesteros, E., 1991a. Seasonality of growth and production of a deep-water population of *Halimeda tuna* (Chlorophyceae, Caulerpales) in the north-western Mediterranean. *Botanica Marina* 34: 291–301.
- Ballesteros, E., 1991b. Structure of a deep-water community of *Halimeda tuna* (Chlorophyceae, Caulerpales) from the North-Western Mediterranean. *Collectanea Botanica* 20: 5–21.
- Barry, S. C., T. K. Frazer & C. A. Jacoby, 2013. Production and carbonate dynamics of *Halimeda incrassata* (Ellis) Lamouroux altered by *Thalassia testudinum* Banks and Soland ex König. *Journal of Experimental Marine Biology and Ecology* 444: 73–80.
- Bilgin, S. & Ö. O. Ertan, 2002. Selected chemical constituents and their seasonal variations in *Flabellia petiolata* (Turra) Nizam. and *Halimeda tuna* (Ellis & Sol.) J.V.Lamour. in the Gulf of Antalya (North-eastern Mediterranean). *Turkish Journal of Botany* 26: 87–90.
- Böhm, E. L., 1973. Studies on the mineral content of calcareous algae. *Bulletin of Marine Science* 23: 177–190.
- Bonacci, O., D. Bonacci, M. Patekar & M. Pola, 2021. Increasing trends in air and sea surface temperature in the Central Adriatic Sea (Croatia). *Journal of Marine Science and Engineering* 9: 1–17.
- Borowitzka, M. A. & A. W. D. Larkum, 1976. Calcification in the green alga *Halimeda*. II. The exchange of Ca^{2+} and the occurrence of age gradients in calcification and photosynthesis. *Journal of Experimental Botany* 27: 864–878.
- Borowitzka, M. A. & A. W. D. Larkum, 1987. Calcification in algae: mechanisms and the role of metabolism. *Critical Reviews in Plant Sciences* 6: 1–45.
- Canals, M. & E. Ballesteros, 1997. Production of carbonate particles by phytobenthic communities on the Mallorca-Menorca shelf, northwestern Mediterranean Sea. *Deep-Sea Research II* 44: 611–629.
- Cardini, A., K. Seetah & G. Barker, 2015. How many specimens do I need? Sampling error in geometric morphometrics: testing the sensitivity of means and variances in simple randomized selection experiments. *Zoomorphology* 134: 149–163.
- Carneiro, P. B. M., J. U. Pereira & H. Matthews-Cascon, 2018. Standing stock variations, growth and CaCO_3 production by the calcareous green alga *Halimeda opuntia*. *Journal of the Marine Biological Association of the United Kingdom* 98: 401–409.

- Davies, P. J., 2011. *Halimeda* bioherms. In Hopley, D. (ed), *Encyclopedia of Modern Coral Reefs* Springer, Dordrecht: 539–549.
- Drew, E. A., 1983. *Halimeda* biomass, growth rates and sediment generation on reefs in the Central Great Barrier Reef Province. *Coral Reefs* 2: 101–110.
- Gunz, P. & P. Mitteroecker, 2013. Semilandmarks: a method for quantifying curves and surfaces. *Hystrix Italian Journal of Mammalogy* 24: 103–109.
- Habel, K., R. Grasman, R. B. Gramacy, P. Mozharovskiy & D. C. Sterratt, 2019. geometry: mesh generation and surface tessellation. R package version 0.4.5. <https://CRAN.R-project.org/package=geometry>
- Hall-Spencer, J. M. & B. P. Harvey, 2019. Ocean acidification impacts on coastal ecosystem services due to habitat degradation. *Emerging Topics in Life Sciences* 3: 197–206.
- Hammer, Ø., D. A. T. Harper & P. D. Ryan, 2001. PAST: paleontological statistics software package for education and data analysis. *Palaeontologia Electronica* 4: 1–9.
- Hillis, L., 1991. Recent calcified Halimedaceae. In Riding, R. (ed), *Calcareous Algae and Stromatolites* Springer, Heidelberg: 167–188.
- Hillis-Colinvaux, L., 1980. *Ecology and Taxonomy of Halimeda: Primary Producer of Coral Reefs*, Academic Press, London:
- Jensen, P. R., R. A. Gibson, M. M. Littler & D. S. Littler, 1985. Photosynthesis and calcification in four deep-water *Halimeda* species (Chlorophyceae, Caulerpales). *Deep-Sea Research* 32: 451–464.
- Klingenberg, C. P., M. Barluenga & A. Meyer, 2002. Shape analysis of symmetric structures: quantifying variation among individuals and asymmetry. *Evolution* 56: 1909–1920.
- Kooistra, W. H. C. F. & H. Verbruggen, 2005. Genetic patterns in the calcified tropical seaweeds *Halimeda opuntia*, *H. distorta*, *H. hederacea*, and *H. minima* (Bryopsidales, Chlorophyta) provide insights in species boundaries and interoceanic dispersal. *Journal of Phycology* 41: 177–187.
- Llobet, I., J. M. Gili & R. G. Hughes, 1991. Horizontal, vertical and seasonal distributions of epiphytic hydrozoa on the alga *Halimeda tuna* in the Northwestern Mediterranean Sea. *Marine Biology* 110: 151–159.
- McNicholl, C., M. S. Koch & L. C. Hofmann, 2019. Photosynthesis and light-dependent proton pumps increase boundary layer pH in tropical macroalgae: a proposed mechanism to sustain calcification under ocean acidification. *Journal of Experimental Marine Biology and Ecology* 521: 151208.
- Mucci, A., 1983. The solubility of calcite and aragonite in seawater at various salinities, temperatures, and one atmosphere total pressure. *American Journal of Science* 283: 780–799.
- Neustupa, J. & Y. Nemcova, 2018. Morphological allometry constrains symmetric shape variation, but not asymmetry, of *Halimeda tuna* (Bryopsidales, Ulvophyceae) segments. *PLoS ONE* 13: e0206492.
- Neustupa, J. & Y. Nemcova, 2020. Morphometric analysis of surface utricles in *Halimeda tuna* (Bryopsidales, Ulvophyceae) reveals variation in their size and symmetry within individual segments. *Symmetry* 12: 1271.
- Ortegón-Aznar, I., A. Chuc-Contreras & L. Collado-Vides, 2017. Calcareous green algae standing stock in a tropical sedimentary coast. *Journal of Applied Phycology* 29: 2685–2693.
- Pastor, F., J. A. Valiente & J. L. Palau, 2018. Sea surface temperature in the Mediterranean: trends and spatial patterns (1982–2016). *Pure and Applied Geophysics* 175: 4017–4029.
- Peach, K. E., M. S. Koch, P. L. Blackwelder, D. Guerrero-Given & N. Kamasawa, 2017. Primary utricle structure of six *Halimeda* species and potential relevance for ocean acidification tolerance. *Botanica Marina* 60: 1–11.
- Perez, S. I., V. Bernal & P. N. Gonzalez, 2006. Differences between sliding semilandmark methods in geometric morphometrics, with an application to human craniofacial and dental variation. *Journal of Anatomy* 208: 769–784.
- Perrett, J. J. & D. J. Mundfrom, 2010. Bonferroni procedure. In Salkind, N. J. (ed), *Encyclopedia of Research Design* Sage Publ, Thousand Oaks, CA: 98–101.
- Pongparadon, S., G. C. Zuccarello & A. Prathep, 2017. High morpho-anatomical variability in *Halimeda macroloba* (Bryopsidales, Chlorophyta) in Thai waters. *Phycological Research* 65: 136–145.
- Pongparadon, S., S. Nooek & A. Prathep, 2020. Phenotypic plasticity and morphological adaptation of *Halimeda opuntia* (Bryopsidales, Chlorophyta) to light intensity. *Phycological Research* 68: 115–125.
- Prathep, A., R. Kaewsrihaw, J. Mayakun & A. Darakrai, 2018. The effects of light intensity and temperature on the calcification rate of *Halimeda macroloba*. *Journal of Applied Phycology* 30: 3405–3412.
- Prát, S. & J. Hamáčková, 1946. The analysis of calcareous marine algae. *Studia Botanica Československa* 7: 112–126.
- R Core Team, 2020. *A Language and Environment for Statistical Computing*, R Foundation for Statistical Computing, Vienna:
- Rees, S. A., B. N. Opdyke, P. A. Wilson & T. J. Henstock, 2007. Significance of *Halimeda* bioherms to the global carbonate budget based on a geological sediment budget for the Northern Great Barrier Reef, Australia. *Coral Reefs* 26: 177–188.
- Rindi, F., M. M. Pasella, M. F. E. Lee & H. Verbruggen, 2020. Phylogeography of the mediterranean green seaweed *Halimeda tuna* (Ulvophyceae, Chlorophyta). *Journal of Phycology* 56: 1109–1113.
- Rohlf, F. J., 2015. The tps series of software. *Hystrix Italian Journal of Mammalogy* 26: 9–12.
- Schaefer, K., T. Lauc, P. Mitteroecker, P. Gunz & F. L. Bookstein, 2006. Dental arch asymmetry in an isolated Adriatic community. *American Journal of Physical Anthropology* 129: 132–142.
- Smith, J. E., C. M. Smith, P. S. Vroom, K. L. Beach & S. Miller, 2004. Nutrient and growth dynamics of *Halimeda tuna* on Conch Reef, Florida Keys: possible influence of internal tides on nutrient status and physiology. *Limnology and Oceanography* 49: 1923–1936.
- Stark, L. M., L. Almodovar & R. W. Krauss, 1969. Factors affecting the rate of calcification in *Halimeda opuntia* (L.) Lamouroux and *Halimeda discoidea* Decaisne. *Journal of Phycology* 5: 305–312.

- van Tussenbroek, B. I. & J. K. van Dijk, 2007. Spatial and temporal variability in biomass and production of psammothytic *Halimeda incrassata* (Bryopsidales, Chlorophyta) in a Caribbean reef lagoon. *Journal of Phycology* 43: 69–77.
- Verbruggen, H., O. De Clerck & E. Coppejans, 2005. Deviant segments hamper a morphometric approach towards *Halimeda* taxonomy. *Cryptogamie Algologie* 26: 259–274.
- Verbruggen, H., O. De Clerck, A. D. R. N'yeurt, H. Spalding & P. S. Vroom, 2006. Phylogeny and taxonomy of *Halimeda incrassata*, including descriptions of *H. kanaloana* and *H. heteromorpha* spp. nov. (Bryopsidales, Chlorophyta). *European Journal of Phycology* 41: 337–362.
- Vergés, A., P. D. Steinberg, M. E. Hay, A. G. B. Poore, A. H. Campbell, E. Ballesteros, K. L. Heck Jr., D. J. Booth, M. A. Coleman, D. A. Feary, W. Figueira, T. Langlois, E. M. Marzinelli, T. Mizerek, P. J. Mumby, Y. Nakamura, M. Roughan, E. Van Sebille, A. S. Gupta, D. A. Smale, F. Tomas, T. Wernberg & S. K. Wilson, 2014. The tropicalization of temperate marine ecosystems: climate-mediated changes in herbivory and community phase shifts. *Proceedings of the Royal Society B* 281: 20140846.
- Vroom, P. S., C. M. Smith, J. A. Coyer, L. J. Walters, C. L. Hunter, K. S. Beach & J. E. Smith, 2003. Field biology of *Halimeda tuna* (Bryopsidales, Chlorophyta) across a depth gradient: comparative growth, survivorship, recruitment, and reproduction. *Hydrobiologia* 501: 149–166.
- Wizemann, A., F. W. Meyer & H. Westphal, 2014. A new model for the calcification of the green macro-alga *Halimeda opuntia* (Lamouroux). *Coral Reefs* 33: 951–964.
- Yñiguez, A. T., J. W. McManus & L. Collado-Vides, 2010. Capturing the dynamics in benthic structures: environmental effects on morphology in the macroalgal genera *Halimeda* and *Dictyota*. *Marine Ecology Progress Series* 411: 17–32.

Publisher's Note Springer Nature remains neutral with regard to jurisdictional claims in published maps and institutional affiliations.